

## Analysis of the moving-photocARRIER-grating technique for the determination of mobility and lifetime of photocarriers in semiconductors

U. Haken, M. Hundhausen, and L. Ley

*Institut für Technische Physik, Universität Erlangen-Nürnberg, Erwin-Rommel-Straße 1, D-91058 Erlangen, Germany*

(Received 28 October 1994)

We describe a technique for the determination of the carrier lifetime ( $\tau$ ) and the carrier mobilities ( $\mu_n, \mu_p$ ) in semiconductors, namely, the moving-photocARRIER-grating method. This technique utilizes a moving intensity grating that is generated by the superposition of frequency shifted laser beams for the illumination of the sample. This results in a spatial *and* temporal modulation of the generation rate of photoelectrons and holes and, as a consequence, in a modulation of the photocARRIER densities. The amplitudes and phases of the resulting carrier densities, space charges, and electric fields are calculated by solving the continuity and Poisson equations in the small signal approach. Their dependence on grating velocity and grating period are analyzed in the lifetime and the relaxation-time regimes. It is shown that a dc short circuit current  $j_{sc}$  results from the action of space charge induced fields on the photogenerated electrons and holes that can be measured in an external circuit. The validity of this analysis is demonstrated by comparing the expression for  $j_{sc}$  with data obtained for two *a*-Si:H samples that realize the lifetime and the relaxation-time regimes, respectively. Good fits are obtained over a wide range of grating periods and grating velocities for material parameters  $\mu_n$ ,  $\mu_p$ , and  $\tau$  that compare favorably with values obtained from other measurements.

### I. INTRODUCTION

The mobilities and the common lifetime of electrons and holes in semiconductors are important parameters that determine the performance of many devices, such as solar cells or thin film transistors. There is a class of experiments which rely on the spatial and sometimes also the temporal evolution of a carrier distribution that is initially nonuniform. The oldest such method is the Haynes-Shockley experiment in which a light spot is used to excite a photocARRIER distribution that drifts in an external applied electric field.<sup>1</sup>

Ritter, Zeldov, and Weiser have introduced the steady-state photocARRIER-grating (SSPG) technique for the determination of the ambipolar diffusion length ( $L_{amb}$ ) in semiconductors.<sup>2,3</sup> This technique is now widely used for amorphous silicon.<sup>4-7</sup> In the SSPG technique a sample is illuminated by two coherent laser beams which form a sinusoidal light intensity pattern with a spatial period  $\Lambda$ . The conductivity of the sample is measured perpendicular to the grating and compared to the conductivity for homogeneous illumination. From the evaluation of the different conductivities as a function of  $\Lambda$  the apparent diffusion length  $L_{app}$  is obtained. Ritter *et al.* have shown that space charges have to be taken into account when the ambipolar diffusion length is to be calculated from  $L_{app}$ .<sup>8</sup>

A drawback of the SSPG method is the fact that the ambipolar diffusion length is the square root of the product of lifetime and ambipolar diffusion constant. Hence, due to the lack of temporal information, SSPG does not allow a separate measurement of lifetime and ambipolar mobility. Consequently, SSPG is often combined with time resolved measurements of the photoconductivity to

determine the carrier lifetime.

The transient grating (TG) technique introduces the temporal aspect by employing a short laser pulse for the generation of spatially modulated photocARRIER densities.<sup>9,10</sup> Their spatiotemporal development is monitored by the time resolved measurement of the diffraction intensity of a second laser beam. The decay of the modulated carrier densities in this case is a combined effect of the blurring of the photocARRIER grating by diffusion and the simultaneous decay by recombination. Performing these measurements as a function of grating period yields the ambipolar diffusion constant  $D$  and the photocARRIER lifetime  $\tau$ . However, the concentration of photocARRIERS created by the single laser pulses are usually well above the densities encountered in normal device operation and the material parameters derived by this method might thus not be relevant for this purpose.

Hattori *et al.* measured the frequency dependent photoconductivity using a laser interference grating whose amplitude is temporally modulated.<sup>11</sup> The size of the intensity used by Hattori is of the same order as that usually used in device operation. Combining this with conventional (i.e., without illumination by the interference grating) frequency resolved photoconductivity measurements, Hattori was also able to obtain carrier mobilities and lifetime.

We have recently extended the SSPG technique by using a *moving* interference grating for illumination resulting in a moving photocARRIER grating (MPG).<sup>12,13</sup> This introduces the temporal aspect that is lacking in the SSPG technique. We have demonstrated that with this technique the mobilities and the lifetime of electrons and holes can be determined individually from a measurement of the short circuit current as a function of the

velocity  $v_{gr}$  and the spatial period  $\Lambda$  of the intensity grating. The short circuit current is closely related to space charges and the electric fields accompanying them and we show in this paper how the space charges evolve when the intensity grating moves. For that purpose we calculate the amplitude of the modulated electron and hole distributions and their phase shift relative to the intensity grating. We show that for the standing grating the electric fields connected with the space charges are out of phase by  $\pi/2$  with the photocarrier densities. Due to this fact no net current is measured in this case. For a moving grating, however, there is a phase shift between electron and hole distributions resulting in a component of the electric field which is in phase with the modulated photocarrier densities. This configuration gives thus a current without an external field. The very existence of the experimentally observed short circuit current requires different electron and hole mobilities and the absolute value and its sign makes the separate evaluations of  $\mu_n$  and  $\mu_p$  possible.

Our experiment has some relation to the experiment of Trofimov and Stepanov who use an interference grating of sub-band-gap light that vibrates with a small amplitude, resulting in an ac current that is measured time resolved.<sup>14</sup> The MPG experiment is different from their experiment firstly because we use a continuously moving laser interference grating and secondly because Trofimov and Stepanov use the laser light for the excitation of electrons from deep defects rather than for the creation of free electrons and holes.

The MPG experiment discussed in this paper does not require the high photocarrier densities of the TG experiment. The temporal aspect is realized by the translation of the intensity grating without changing its modulation amplitude. Photocarrier mobilities and lifetime can thus be extracted from the measured dc short circuit current without the need to combine this measurement with time or frequency resolved measurements of the photoconductivity.

In previous papers on the MPG technique we have demonstrated its applicability for the determination of the material parameters without detailed discussion of the underlying theory.<sup>12,13,15</sup> This paper is in order to present this theory and to give a comparative analysis of measurements on highly<sup>12,15</sup> and weakly<sup>13</sup> photoconducting samples.

The paper is organized as follows. In Sec. II the experimental setup and the samples used for this study are described. The theory for the evaluation of the experimental data is given in Sec. III. The results of that section are analyzed separately for the lifetime regime and for the relaxation-time regime in Sec. IV, and in Sec. V we apply our method to the determination of the material parameters of two specimen of amorphous silicon in the two different regimes.

## II. EXPERIMENTAL DETAILS

### A. Setup for the MPG method

The experimental setup used for the MPG method is shown in Fig. 1. Except for the acousto-optic modulators

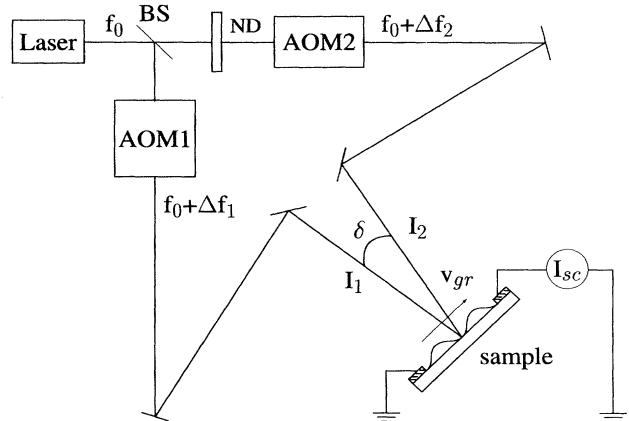


FIG. 1. Experimental setup for the moving photo-carrier-grating (MPG) technique. The HeNe laser beam ( $\hbar\omega = 1.96$  eV) is split into two parts by means of a beam splitter (BS). These are frequency shifted by the use of acousto-optic modulators in order to impress a frequency difference on the two laser beams that interfere at the sample surface. This results in a intensity grating that moves with a velocity  $v_{gr}$  along the surface.

(AOM's) it is similar to the arrangement used for the SSPG technique: A laser beam (wavelength  $\lambda$ ) is split into two parts which interfere at the surface of the sample under an angle  $\delta$ . Thus, an intensity grating with spatial period  $\Lambda = \lambda/[2 \sin(\delta/2)]$  is created. The modulation of this grating can be made small using a neutral density filter to attenuate one beam. Deviating from the SSPG experiment we use two AOM's that shift the frequencies of the laser beams by  $\Delta f_1$  and  $\Delta f_2$ , respectively. The resulting frequency difference  $\Delta f = \Delta f_1 - \Delta f_2$  causes the intensity grating to move with a velocity  $v_{gr} = \Lambda \Delta f$  along the sample surface. The intensity at the sample surface (the  $x$  coordinate) is given by

$$I(x, t) = I_0 + \Delta I(x, t) = I_0 + I_m \cos [k(x - v_{gr}t)]. \quad (1)$$

Here,  $k$  is the spatial frequency ( $k = 2\pi/\Lambda$ ). The homogeneous part  $I_0$  and the amplitude of the modulated part  $I_m$  of the intensity are related to the intensities  $I_1$  and  $I_2$  of the two interfering laser beams according to

$$I_0 = I_1 + I_2, \quad I_m = 2\sqrt{I_1 I_2}. \quad (2)$$

The experimental quantity that we measure in this experiment is the dc short circuit current that is induced in the sample as a result of the moving intensity grating. The short circuit current is typically in the  $10^{-12}$  A range and we use an electrometer to measure this current.

### B. Samples

We investigated two samples in order to study two different regimes. In the lifetime regime the recombination

lifetime of photogenerated carriers  $\tau$  is longer than the dielectric relaxation time  $\tau_{\text{diel}}$  that is determined by the conductivity  $\sigma$  and the dielectric constant  $\epsilon$  of the sample ( $\tau_{\text{diel}} = \epsilon\epsilon_0/\sigma$ ). The relaxation-time regime exists if on the other hand  $\tau_{\text{diel}} \gg \tau$ . The lifetimes of the samples were determined as explained in Sec. V.

Undoped amorphous hydrogenated silicon (*a*-Si:H) measured at room temperature served as a sample for the lifetime regime; at a light intensity of 10 mW/cm<sup>2</sup> this sample had  $\tau/\tau_{\text{diel}} \approx 10$ . For the relaxation-time regime study we used an *n*-type sample and measured at 120 K. At 80 mW/cm<sup>2</sup> this sample had  $\tau/\tau_{\text{diel}} \approx 0.025$ .

The samples were prepared with plasma enhanced chemical vapor deposition under conditions that yield device quality films. Before the measurements, the samples were light soaked (20 h with 150 mW/cm<sup>2</sup> heat filtered light) in order to avoid any changes of the sample properties during the measurements.<sup>16</sup>

### III. THEORY

We treat the problem of the MPG in a manner similar to previous papers dealing with SSPG.<sup>4,8,17,18</sup> The spatial modulation of the photogenerated electron and hole distributions is considered by taking into account the inhomogeneous generation rate as well as the diffusion, drift, and recombination of the carriers following their generation. In order to describe the case of the moving photocarrier grating we have to replace the spatially modulated but temporarily steady generation rate of the SSPG by a time dependent generation rate:

$$G(x, t) = G_0 + \Delta G(x, t) = G_0 + g \cos [k(x - v_{\text{gr}}t)]. \quad (3)$$

Here, the amplitude of the modulation of the generation rate  $g$  relates to the quantity  $I_m$  in Eq. (1), whereas  $G_0$  relates to the homogeneous part of the intensity  $I_0$ . We are going to calculate in the one-dimensional approximation the space and time dependent electron and hole densities,  $N(x, t)$  and  $P(x, t)$ , respectively. The continuity equations for these quantities are

$$\frac{\partial N(x, t)}{\partial t} = \frac{1}{e} \frac{\partial j_n(x, t)}{\partial x} + G(x, t) - R(x, t), \quad (4)$$

$$\frac{\partial P(x, t)}{\partial t} = -\frac{1}{e} \frac{\partial j_p(x, t)}{\partial x} + G(x, t) - R(x, t), \quad (5)$$

where  $R(x, t)$  is the recombination rate. The current densities  $j_n(x, t)$  and  $j_p(x, t)$  are the sum of the respective drift and diffusion currents:

$$j_n(x, t) = e\mu_n(x, t)N(x, t)E(x, t) + eD_n \frac{\partial N(x, t)}{\partial x}, \quad (6)$$

$$j_p(x, t) = e\mu_p(x, t)P(x, t)E(x, t) - eD_p \frac{\partial P(x, t)}{\partial x}, \quad (7)$$

where  $E(x, t)$  is the electric field. For crystalline semiconductors  $N(x, t)$  and  $P(x, t)$  are the respective free

carrier densities. In noncrystalline semiconductors, the class of materials used for the measurements here, any photogenerated carrier might in general experience multiple trapping before its recombination. Thus,  $N(x, t)$  and  $P(x, t)$  include *free* and *trapped* photocarriers in the case of noncrystalline semiconductors which have a high density of localized states extending from the band edges into the gap. Moreover, the mobilities  $\mu_n$  and  $\mu_p$  are not the free carrier mobilities, but rather average quantities taking into account the multiple trapping process. In such instances, the mobilities might depend on the carrier densities which is the reason for their space and time dependence in Eqs. (6) and (7). Under these conditions the small signal mobilities  $\mu'_n$  and  $\mu'_p$  differ from the drift mobilities according to<sup>17,19</sup>

$$\mu'_n = \mu_n + N \frac{d\mu_n}{dN}, \quad \mu'_p = \mu_p + P \frac{d\mu_p}{dP}. \quad (8)$$

The effective diffusion constants  $D_n$  and  $D_p$  are related via Einstein's equation to the small signal mobilities  $\mu'_n$  and  $\mu'_p$  rather than to  $\mu_n$  and  $\mu_p$ .<sup>17,20</sup>

$$D_n = \mu'_n \frac{k_B T}{e}, \quad D_p = \mu'_p \frac{k_B T}{e}. \quad (9)$$

Combining Eqs. (4)–(9) we obtain

$$\begin{aligned} \frac{\partial N(x, t)}{\partial t} = & \mu'_n E(x, t) \frac{\partial N(x, t)}{\partial x} + \mu_n N(x, t) \frac{\partial E(x, t)}{\partial x} \\ & + \mu'_n \frac{k_B T}{e} \frac{\partial^2 N(x, t)}{\partial x^2} + G(x, t) - R(x, t), \end{aligned} \quad (10)$$

$$\begin{aligned} \frac{\partial P(x, t)}{\partial t} = & -\mu'_p E(x, t) \frac{\partial P(x, t)}{\partial x} - \mu_p P(x, t) \frac{\partial E(x, t)}{\partial x} \\ & + \mu'_p \frac{k_B T}{e} \frac{\partial^2 P(x, t)}{\partial x^2} + G(x, t) - R(x, t). \end{aligned} \quad (11)$$

For simplicity we set  $\mu_n = \mu'_n$  and  $\mu_p = \mu'_p$  in the following as was done in papers dealing with SSPG<sup>4,8,17</sup> on amorphous semiconductors. This approximation is equivalent to the assumption that the mobilities do not depend on the generation rate [see Eq. (8)]. For crystalline semiconductors  $\mu_{n,p} = \mu'_{n,p}$  is usually fulfilled.

Reformulating Eqs. (10) and (11) for the variations of the relevant physical quantities from their homogeneous values ( $\Delta N = N - N_0$ ,  $\Delta P = P - P_0$ ,  $\Delta R = R - R_0$ , and  $\Delta G = G - G_0$ ), we get

$$\begin{aligned} \frac{\partial \Delta N}{\partial t} = & \mu_n E \frac{\partial \Delta N}{\partial x} + \mu_n N \frac{\partial E}{\partial x} + \mu_n \frac{k_B T}{e} \frac{\partial^2 \Delta N}{\partial x^2} \\ & + \Delta G - \Delta R, \end{aligned} \quad (12)$$

$$\begin{aligned} \frac{\partial \Delta P}{\partial t} = & -\mu_p E \frac{\partial \Delta P}{\partial x} - \mu_p P \frac{\partial E}{\partial x} + \mu_p \frac{k_B T}{e} \frac{\partial^2 \Delta P}{\partial x^2} \\ & + \Delta G - \Delta R. \end{aligned} \quad (13)$$

Here, we used  $R_0 = G_0$  and  $N_0 = P_0$  (global charge neutrality), which is true if the dark carrier densities

are small compared to the photocarrier densities, i.e., if  $\sigma_{\text{dark}} \ll \sigma_{\text{ph}}$ .  $\Delta R$  can be approximated by<sup>17</sup>

$$\Delta R = \frac{1}{2\tau}(\Delta N + \Delta P). \quad (14)$$

Note that for noncrystalline semiconductors  $\tau$  is the total photocarrier recombination lifetime, not the free carrier lifetime. Since electrons recombine with holes, by definition the recombination lifetime of electrons equals that of holes. This also implies  $N_0 = P_0 = G_0\tau$  (see above). The electric field is the sum of the constant, externally applied field  $E_0$  plus the space charge field ( $E = E_0 + E_{\text{sc}}$ ). It is related to the carrier densities via Poisson's equation:

$$\frac{\partial E}{\partial x} = \frac{\partial E_{\text{sc}}}{\partial x} = \frac{e}{\epsilon\epsilon_0}(\Delta P - \Delta N). \quad (15)$$

The coupled differential equations (12), (13), and (15) are difficult to solve, but for weak modulation it is expected that the relevant physical parameters vary sinusoidally as does  $G(x, t)$ . In general, however, they will have variable phase shifts with respect to the phase of the moving generation rate. This is taken into account by introducing complex amplitudes, denoted here by lower case letters ( $n$ ,  $p$ , and  $e_{\text{sc}}$ ):

$$\Delta N(x, t) = \frac{1}{2}\{n(k, v_{\text{gr}}) \exp[-ik(x - v_{\text{gr}}t)] + \text{c.c.}\}, \quad (16)$$

$$\Delta P(x, t) = \frac{1}{2}\{p(k, v_{\text{gr}}) \exp[-ik(x - v_{\text{gr}}t)] + \text{c.c.}\}, \quad (17)$$

$$E_{\text{sc}}(x, t) = \frac{1}{2}\{e_{\text{sc}}(k, v_{\text{gr}}) \exp[-ik(x - v_{\text{gr}}t)] + \text{c.c.}\}, \quad (18)$$

where c.c. is the complex conjugate of the respective preceding term. The complex amplitudes  $n(k, v_{\text{gr}})$ ,  $p(k, v_{\text{gr}})$ , and  $e_{\text{sc}}(k, v_{\text{gr}})$  can also be written in terms of their amplitudes and phases according to  $n(k, v_{\text{gr}}) = |n| \exp(i\varphi_n)$ ,  $p(k, v_{\text{gr}}) = |p| \exp(i\varphi_p)$ , and  $e_{\text{sc}}(k, v_{\text{gr}}) = |e_{\text{sc}}| \exp(i\varphi_e)$ . The differential equations reduce to a set of coupled linear equations for the complex amplitudes where any product between two complex amplitudes is neglected for the weak modulation used here:

$$ikv_{\text{gr}}n = -ik\mu_n E_0 n + \mu_n N_0 \frac{e}{\epsilon\epsilon_0}(p - n) - \mu_n k^2 \frac{k_B T}{e} n + g - \frac{1}{2\tau}(n + p), \quad (19)$$

$$ikv_{\text{gr}}p = +ik\mu_p E_0 p - \mu_p P_0 \frac{e}{\epsilon\epsilon_0}(p - n) - \mu_p k^2 \frac{k_B T}{e} p + g - \frac{1}{2\tau}(n + p). \quad (20)$$

In the following we discuss the case of zero applied external field ( $E_0 = 0$ ). The solutions of Eqs. (19) and (20) are given by (note that  $N_0 = P_0$  is used)

$$n = \frac{a_n + ia_1}{a_2 + ia_3}, \quad p = \frac{a_p + ia_1}{a_2 + ia_3}, \quad (21)$$

where

$$a_n = g \left( k^2 D_p + \frac{eN_0}{\epsilon\epsilon_0}(\mu_n + \mu_p) \right),$$

$$a_p = g \left( k^2 D_n + \frac{eN_0}{\epsilon\epsilon_0}(\mu_n + \mu_p) \right),$$

$$a_1 = gkv_{\text{gr}},$$

$$a_2 = \frac{1}{\tau} \frac{eN_0}{\epsilon\epsilon_0}(\mu_n + \mu_p) + \frac{k^2}{2\tau}(D_n + D_p) + k^2 \frac{eN_0}{\epsilon\epsilon_0}(D_p\mu_n + D_n\mu_p) + k^4 D_n D_p - k^2 v_{\text{gr}}^2,$$

$$a_3 = kv_{\text{gr}} \left( k^2(D_n + D_p) + \frac{eN_0}{\epsilon\epsilon_0}(\mu_n + \mu_p) + \frac{1}{\tau} \right). \quad (22)$$

In order to obtain the short circuit current  $j_{\text{sc}}$  the drift currents of the modulated carrier densities have to be averaged over one spatial period  $\Lambda$ :

$$j_{\text{sc}} = \frac{1}{\Lambda} \int_0^\Lambda [e\mu_n N(x, t) + e\mu_p P(x, t)] E(x, t) dx. \quad (23)$$

Note, that the diffusion currents do not contribute to  $j_{\text{sc}}$  because they vanish when averaged over one period. Inserting Eqs. (16)–(18) into Eq. (15) we obtain  $e_{\text{sc}}$  as the solution of Poisson's equation written in its complex form:

$$e_{\text{sc}} = \frac{i}{k} \frac{e}{\epsilon\epsilon_0}(p - n). \quad (24)$$

The integration of  $j_{\text{sc}}$  performed with the complex amplitudes gives

$$j_{\text{sc}}(k, v_{\text{gr}}) = i \frac{e^2(\mu_n + \mu_p)}{4k\epsilon\epsilon_0}(n^*p - np^*) = \frac{e^2(\mu_n + \mu_p)}{2k\epsilon\epsilon_0}|n||p| \sin(\varphi_n - \varphi_p), \quad (25)$$

where \* denotes the complex conjugate. The result for  $j_{\text{sc}}$  finally is

$$j_{\text{sc}}(k, v_{\text{gr}}) = \frac{c_1 v_{\text{gr}}}{c_2 + c_3 v_{\text{gr}}^2 + c_4 v_{\text{gr}}^4}, \quad (26)$$

where the constants  $c_1$ – $c_4$  are given by

$$c_1 = \frac{e^2}{2\epsilon\epsilon_0}(\mu_n + \mu_p)(g\tau)^2 k^2 (D_n - D_p),$$

$$c_2 = \frac{1}{\tau^2} \left[ \left( a + \frac{(b+1)^2}{4b} l^2 \right) (1 + l^2) \right]^2,$$

$$c_3 = k^2 \left( 1 + a^2 + \frac{(b+1)^2 + 2a(b^2+1)}{2b} l^2 + \frac{(b+1)^2(b^2+1)}{4b^2} l^4 \right),$$

$$c_4 = k^4 \tau^2, \quad (27)$$

with the following short-hand notations:

$$a = \frac{\tau}{\tau_{\text{diel}}} = \frac{N_0 e (\mu_n + \mu_p) \tau}{\epsilon \epsilon_0}, \quad b = \frac{\mu_n}{\mu_p},$$

$$D = \frac{2D_n D_p}{D_n + D_p}, \quad l = \sqrt{\tau D k}. \quad (28)$$

#### IV. ANALYSIS

##### A. Modulated carrier densities

Before we analyze the result of Eq. (21), we emphasize that for the MPG the amplitudes of the modulated electron and hole densities  $|n|$  and  $|p|$  differ in general, as do their phases  $\varphi_n$  and  $\varphi_p$  relative to that of the intensity grating. Let us first consider two ideal cases which are generally not realized; in case A we assume  $\varphi_n = \varphi_p$  but  $|n| \neq |p|$ , i.e., electron and hole densities are in phase having different amplitudes. For case B the amplitudes are assumed to be equal ( $|n| = |p|$ ) but the electron density is phase shifted by a small amount with respect to the hole density ( $\varphi_n \neq \varphi_p$ ). These two cases are sketched in Fig. 2, where the carrier densities  $N$  and  $P$ , the space charge density  $\rho$ , the electric field  $E_{sc}$ , and the drift current density  $j_{dr}$  are plotted as a function of the spatial coordinate  $x$ . Let us first discuss case A. If electron and hole densities are in phase [see Fig. 2(a)] the resulting space charge density (b) is also in phase with the carrier densities. The electric field that relates to  $\rho$  via Poisson's

equation (c), however, is out of phase by  $90^\circ$ . The spatially resolved drift current ( $j_{dr} = j_{dr,n} + j_{dr,p}$ ) obtained by multiplying  $E_{sc}$  with the respective carrier densities and their mobilities is plotted in Fig. 2(d). For case A,  $j_{dr}$  varies symmetrically around zero, i.e., its dc component vanishes. This is due to the  $90^\circ$  phase shift between  $E_{sc}$  and the carrier densities.

The situation is different when a phase shift between electron and hole densities exists (case B). In this case the space charge density is shifted by  $-90^\circ$  with respect to the average of electron and hole distributions. As a result,  $E_{sc}$  turns out to be in phase with  $N(x,t)$  and  $P(x,t)$  (note that  $\Delta\varphi_{np} = \varphi_n - \varphi_p$  is assumed to be small). Hence, the drift current density (d) is no longer modulated around zero but contains a finite dc component  $j_{dc}$  which can be measured as a short circuit current in an external circuit.

In conclusion, differences in the amplitudes  $|n|$  and  $|p|$  as well as differences in the phases  $\varphi_n$  and  $\varphi_p$  give rise to internal electric fields; but only the latter give rise to a short circuit current. Therefore we are going to analyze the modulated carrier densities that build up due to the moving intensity grating by discussing  $|n|$  and  $|p|$  as well as  $\varphi_n$  and  $\varphi_p$ . We will do this separately for the lifetime regime and for the relaxationtime regime in the following subsections.

##### 1. Lifetime regime

The undoped sample used for our measurements had mobilities  $\mu_n = 0.077 \text{ cm}^2/\text{V s}$  and  $\mu_p = 0.005 \text{ cm}^2/\text{V s}$  and the recombination lifetime was  $\tau = 2.1 \times 10^{-6} \text{ s}$ . These parameters were obtained from fitting short circuit currents to the theoretical expression derived in Sec. III (see Sec. V below). We use these values and  $\Lambda = 3 \text{ }\mu\text{m}$ ,  $G_0 = 1.8 \times 10^{20} \text{ cm}^{-3} \text{ s}^{-1}$ , and  $g/G_0 = 0.5$  to calculate  $|n|$ ,  $|p|$ ,  $\varphi_n$ , and  $\varphi_p$ . The ratio of lifetime and relaxation time  $a = \tau/\tau_{\text{diel}}$  equals 10 so that the condition for the lifetime regime is fulfilled.

The amplitudes  $|n|$  and  $|p|$  are plotted in Fig. 3. Both

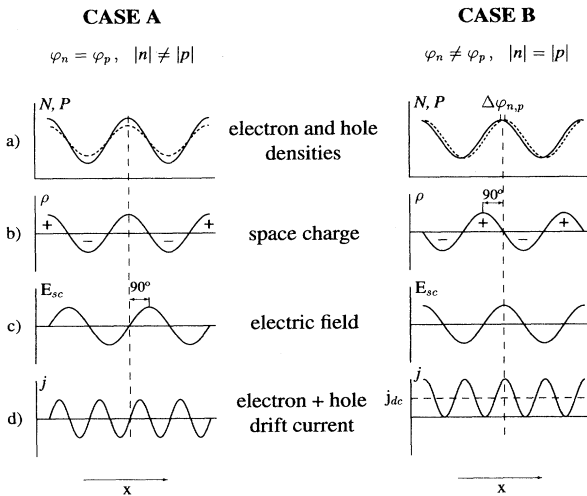


FIG. 2. Sketches of the spatially modulated densities of photogenerated electrons and holes (a), the space charge density  $\rho = e(P - N)$  (b), the electric field resulting from the space charge (c), and the sum of the electron plus hole drift current density (d) as a function of the spatial coordinate  $x$  along the grating. Two situations are depicted: case A corresponds to different amplitudes of electron and hole densities and equal phases, whereas case B is the situation when the phases are different but the amplitudes are equal. Note that the dc current density is zero for case A and nonzero for case B.

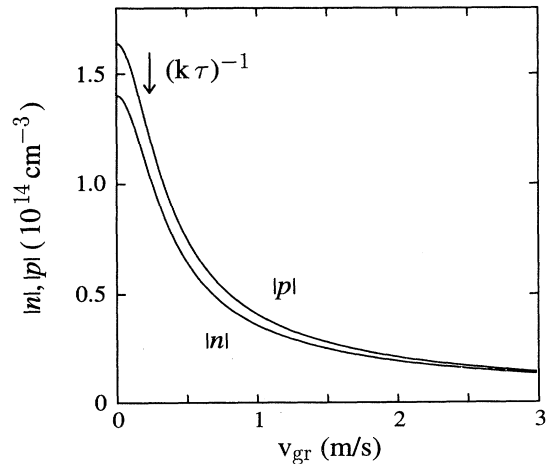


FIG. 3. Amplitudes of the electron and hole densities  $|n|$  and  $|p|$  as derived from Eq. (21) as a function of  $v_{gr}$  for the lifetime regime. The material parameters of the undoped sample of *a*-Si:H were used.

$|n|$  and  $|p|$  decrease with increasing  $v_{gr}$ . This is understood by considering the blurring of the photocarrier grating if the intensity grating changes over times short compared with  $\tau$ . The criterion for a significant blurring is that the amount by which the grating moves during the time  $\tau$  is of the order of the grating period ( $v_{gr}\tau \approx \Lambda$ ). The point where  $v_{gr} = (\tau k)^{-1}$  is marked with an arrow in Fig. 3.

The phases of the electron and hole distributions relative to the phase of the generation rate are plotted in Fig. 4. For a standing grating ( $v_{gr}=0$ ) electrons and holes are in phase with the generation rate, whereas both distributions start to lack behind the generation rate with increasing  $v_{gr}$ . Eventually, for increasing  $v_{gr}$  a phase shift of  $-\pi/2$  is approached.

From Figs. 3 and 4 it can be seen that both amplitudes and phases differ for electrons and holes. Due to the smaller hole diffusion constant the amplitude of the hole distribution is larger than that for the electrons and deviates by the largest amount for small values of  $v_{gr}$ . The phase difference  $\Delta\varphi_{np} = \varphi_n - \varphi_p$ , however, increases over the range of the velocities shown and the electron distribution appears to be closer to the generation rate. In Fig. 5 these differences are plotted vs  $v_{gr}$ . The quantity  $\gamma_{rel} = 2(|p| - |n|)/(|p| + |n|)$ , which is the difference of  $|p|$  and  $|n|$ , normalized to their average, decreases with increasing  $v_{gr}$ .  $\Delta\varphi_{np}$ , however, increases from zero to a broad maximum around  $v_{gr}=2.4$  m/s. This velocity coincides roughly with the velocity defined by  $v_{gr} = (\tau_{diel}k)^{-1}$ , a fact that will be discussed below.

According to the discussion of Fig. 2 both quantities ( $\gamma_{rel}$  and  $\Delta\varphi_{np}$ ) plotted in Fig. 5 give rise to a space charge field: if  $\Delta\varphi_{np}$  were zero, the electric field would be shifted by  $\pi/2$  with respect to  $n$  or  $p$  as is obvious from the imaginary constant on the right hand side of Eq. (24). The amplitude of the field  $|e_{sc}|$  is in this case

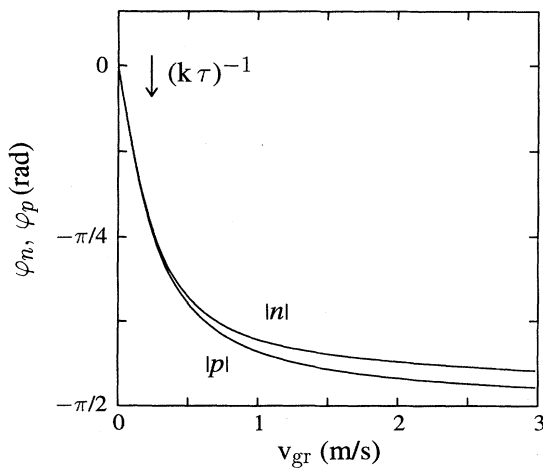


FIG. 4. Phases of the electron and hole distributions  $\varphi_n$  and  $\varphi_p$  as derived from Eq. (21) as a function of  $v_{gr}$  for the lifetime regime.

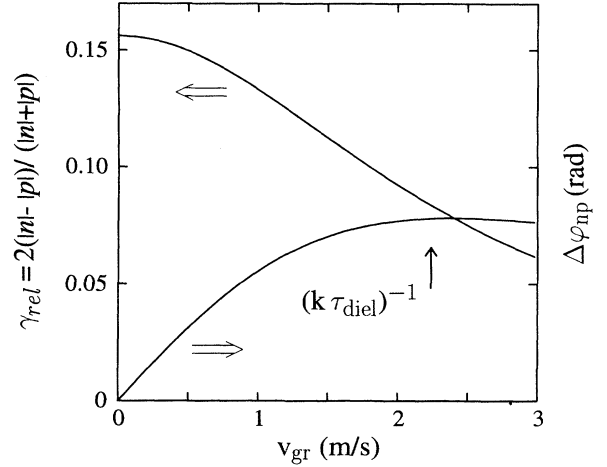


FIG. 5. Normalized difference between absolute electron and hole amplitudes [ $\gamma_{rel} = 2(|p| - |n|)/(|p| + |n|)$ ] (left scale) and difference between electron and hole phases ( $\Delta\varphi_{np} = \varphi_n - \varphi_p$ ) (right scale) as a function of  $v_{gr}$  calculated from the data shown in Figs. 3 and 4.

proportional to  $\gamma_{rel}(|n| + |p|)$  [see Eq. (24)]. If, on the other hand,  $|n|$  and  $|p|$  are equal, the electric field is in phase with the average of the electron and hole densities, i.e.,  $\varphi_e = \overline{\varphi_{np}} = (\varphi_n + \varphi_p)/2$ . The amplitude  $|e_{sc}|$  in this case is proportional to  $\Delta\varphi_{np}(|n| + |p|)$ .

The amplitude  $|e_{sc}|$  and the phase of the space charge field with respect to the average electron and hole phase  $\varphi_e - \overline{\varphi_{np}}$  was calculated from the modulated carrier densities. These quantities are plotted in Figs. 6(a) and 6(b), respectively. The electric field amplitude is largest ( $\approx 170$  V/cm) for  $v_{gr} = 0$  and decreases approximately as  $|n|$  and  $|p|$ . From Fig. 6(b) it is clear that a transition

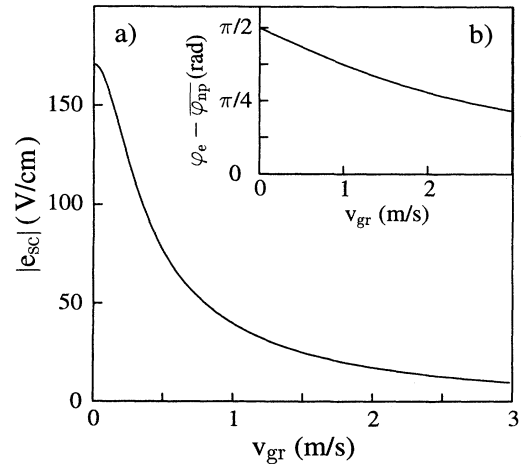


FIG. 6. (a) Amplitude of the electric field as a function of  $v_{gr}$ . (b) Difference between the phase of the electric field  $\varphi_e$  and the average phase  $\overline{\varphi_{np}}$  of modulated electron and hole densities in the lifetime regime.

between a situation where the electric field is shifted by  $\pi/2$  for  $v_{\text{gr}} = 0$  to a situation where the electric field is in phase with the carrier densities occurs. According to the discussion of Fig. 2 this corresponds to the transition from case A ( $|n| \neq |p|$ ) to case B ( $\varphi_n \neq \varphi_p$ ).

## 2. Relaxation-time regime

In this section we are going to discuss the case of the  $n$ -doped sample that was measured at 120 K. The basis of the following discussion are the parameters  $\mu_n = 2.6 \times 10^{-6} \text{ cm}^2/\text{V s}$ ,  $\mu_n/\mu_p=100$ , and  $\tau=5 \times 10^{-6} \text{ s}$ . These parameters are again those obtained in Sec. V. At a light intensity of  $80 \text{ mW/cm}^2$  (corresponding to  $G_0=2 \times 10^{21} \text{ cm}^{-3} \text{ s}^{-1}$ ), the ratio of lifetime and dielectric relaxation time is  $a=0.025$  in this case, so that the relaxation-time regime is realized. Moreover, the experimental parameters  $\Lambda=0.4 \text{ }\mu\text{m}$  and  $g/G_0 = 0.57$  were used. The amplitudes  $|n|$  and  $|p|$  are shown in Fig. 7 as a function of  $v_{\text{gr}}$ . For the following discussion we divide the velocity range into three regimes: In regime I the intensity grating changes on a time scale long compared to  $\tau_{\text{diel}}$ , i.e.,  $v_{\text{gr}} < (k\tau_{\text{diel}})^{-1}$ , whereas in regime II it changes on a time scale shorter than  $\tau_{\text{diel}}$  but still long compared to the lifetime  $\tau$  [ $(k\tau_{\text{diel}})^{-1} < v_{\text{gr}} < (k\tau)^{-1}$ ]. In regime III we have  $v_{\text{gr}} > (k\tau)^{-1}$ . The inset of Fig. 7 depicts regime I and its transition to II on expanded scale. Except for the different scale used for the velocity axis, the overall dependence of the amplitudes shown in Fig. 7 is similar to the case of the lifetime regime (see Fig. 3). That is,  $|n|$  and  $|p|$  decrease with increasing velocity due to the blurring effect when the intensity grating moves. The relevant scale on which this happens is again defined by  $v_{\text{gr}}=(k\tau)^{-1}$  (see the arrow). However, in con-

trast to the lifetime regime (Fig. 3)  $|n|$  and  $|p|$  are equal for sufficiently high velocities (regimes II and III). This is no longer the case for small velocities, as shown in the inset of Fig. 7. The amplitudes deviate in opposite directions from a curve that was extrapolated from higher  $v_{\text{gr}}$  (dashed line in Fig. 7). For  $v_{\text{gr}} = 0$  the extrapolation equals  $g\tau$ , i.e., the modulation amplitude of the generation rate multiplied with the lifetime. For a nonmoving grating the average density  $[(|n|+|p|)/2]$  is determined by the equilibrium between generation and recombination rates. This is so because in the relaxation-time regime the drift and diffusion rates of Eqs. (4) and (5) are small compared to  $R$  and  $G$ . Due to the faster diffusion of the electrons compared to the holes,  $|n|$  is reduced from  $g\tau$  while  $|p|$  increases by as much to keep the recombination rate unchanged [note that  $\Delta R = (\Delta N + \Delta P)/2\tau$  from Eq. (14)]. The difference between  $|n|$  and  $|p|$  is largest for a nonmoving intensity grating ( $v_{\text{gr}} = 0$ ), as is the space charge. If, however, the intensity grating moves on a time scale of the order of the dielectric relaxation time the diffusion-drift equilibrium can no longer be fully established. As a consequence, the difference between  $|n|$  and  $|p|$  is reduced with increasing velocity, i.e., when regime II is reached, as can be seen in the inset of Fig. 7.

It is instructive to compare the velocity dependence of the photocarrier amplitudes with their time dependence after a modulated part of the the generation rate is switched on at a certain time. We have analytically solved the corresponding rate equations in order to obtain  $|n|$  and  $|p|$  as a function of time. For the same parameters as those used in Fig. 7, in particular  $\tau/\tau_{\text{diel}}=0.025$ , the result is shown in Fig. 8. Initially, the buildup of the photocarrier amplitudes occurs exponentially towards a saturation value of  $g\tau$  with a time constant close to  $\tau$ . This is due to the generation and recombination terms in the rate equations. As long as the time is short compared to  $\tau_{\text{diel}}$ ,  $|n|$  and  $|p|$  differ little. For increasing time, however, electron and hole amplitudes depart from  $g\tau$  in opposite directions, due to their different diffusion constants. The time scale on which this happens is defined by  $\tau_{\text{diel}}$ , because the evolution of space charges occurs on

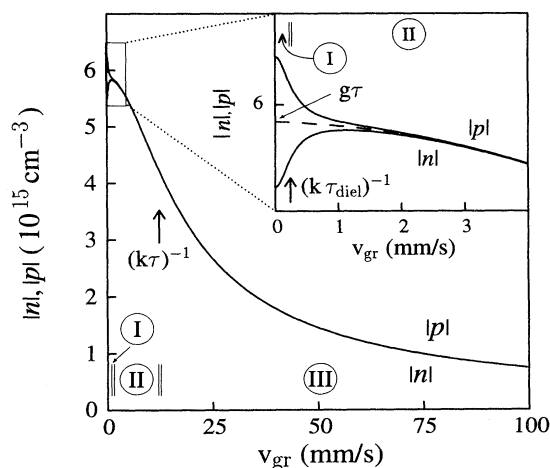


FIG. 7. Amplitude of the electron and hole densities  $|n|$  and  $|p|$  as derived from Eq. (21) as a function of  $v_{\text{gr}}$  for the relaxation-time regime. The material parameters of the  $n$ -doped sample of  $a$ -Si:H at 120 K were used. The inset gives an expanded plot for small velocities. Note the different regimes I–III. For details see text.

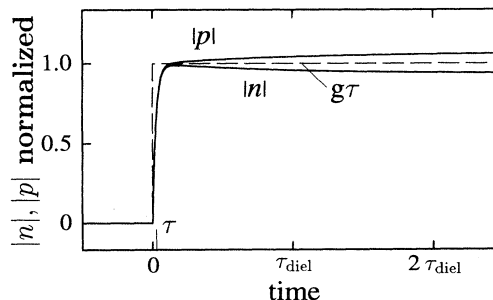


FIG. 8. Buildup of photocarrier grating amplitudes  $|n|$  and  $|p|$  in the relaxation-time regime after a modulated component of the generation rate has been switched on at  $t=0$ .  $|n|$  and  $|p|$  approach  $g\tau$  exponentially with a time constant equal to the recombination lifetime. Due to diffusion  $|n|$  and  $|p|$  start to deviate from each other with a time constant equal to  $\tau_{\text{diel}}$ .

this time scale. Note the complementary roles of grating velocity in Fig. 7 and time in Fig. 8. Immediately after the grating is switched on  $|n|$  and  $|p|$  are small, a situation that corresponds to the blurring of the photocarrier grating when  $v_{gr} \gg (k\tau)^{-1}$  (regime III in Fig. 7). On the other hand, the buildup of space charges that goes along with  $|n| \neq |p|$  requires long times (Fig. 8) or small grating velocities  $v_{gr} < (k\tau_{diel})^{-1}$  (regime I in Fig. 7).

The phases of the electron and hole distributions with respect to the intensity grating,  $\varphi_n$  and  $\varphi_p$ , are plotted in Fig. 9 as a function of  $v_{gr}$ . Again, as for the amplitudes, the overall behavior is similar to the lifetime regime, i.e., for  $v_{gr} = 0$ ,  $\varphi_n$  and  $\varphi_p$  are zero and approach  $-\pi/2$  for large velocities on a scale determined by  $(k\tau)^{-1}$ . In contrast to the case of the lifetime regime the phase difference  $\Delta\varphi_{np}$  is negligibly small for  $v_{gr} \geq (k\tau)^{-1}$  (compare Fig. 7). For small velocities (see the inset of Fig. 9)  $\varphi_n$  and  $\varphi_p$  differ significantly. Although the general trend is that both electron and hole distributions lack behind the intensity grating, this is not true for the electrons for small velocities  $v_{gr} \leq (k\tau_{diel})^{-1}$ ; in this range  $\varphi_n > 0$ , i.e., the electrons move ahead of the intensity grating.

In order to explain this fact, let us consider what happens if the intensity grating is not moving continuously but if its phase is changed from zero to a small finite value at  $t=0$ , i.e., if the grating is displaced by a small positive distance  $\Delta x \ll \Lambda$ . It is obvious that the corresponding photocarrier distributions are in phase with the intensity grating for  $t \leq 0$  and for  $t \rightarrow \infty$  and we consider the dependence of the phases  $\varphi_n$  and  $\varphi_p$  for an intermediate time.

The phase shifted generation rate (for  $t > 0$ ) can be decomposed into cos and sin components:

$$g \cos(kx + k\Delta x) \approx g \cos(kx) + gk\Delta x \sin(kx). \quad (29)$$

This approximation is valid for  $\Delta x \ll \Lambda$ . The discontin-

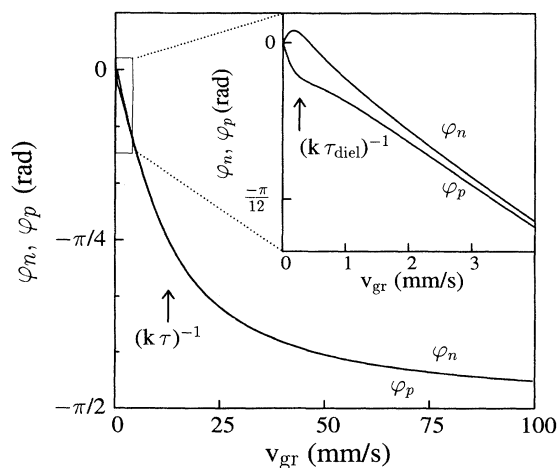


FIG. 9. Phases of the electron and hole distributions  $\varphi_n$  and  $\varphi_p$  as derived from Eq. (21) as a function of  $v_{gr}$  in the relaxation-time regime. The inset shows the same expanded velocity range as that of Fig. 7.

uous phase shift can thus be understood as an additional weak phase shifted generation rate switched on at time  $t = 0$ . The corresponding sin component of the photocarrier distribution consequently builds up as shown in Fig. 8, where the ordinate value  $g\tau$  has to be replaced by  $g\tau k\Delta x$ . As seen in this figure, the sin components of electron and hole distributions are close to  $g\tau k\Delta x$  for a time well above  $\tau$  but still below  $\tau_{diel}$  and we calculate the respective phases for this time. For the cos component, which is the steady-state value of the amplitudes ( $|n|_{(v_{gr}=0)}$ , and  $|p|_{(v_{gr}=0)}$ ) we know from Fig. 7 that the following relation holds:

$$|n|_{(v_{gr}=0)} < g\tau < |p|_{(v_{gr}=0)}. \quad (30)$$

For the electron and hole phases which are to first order the ratios of the respective sin to cos components we get

$$\varphi_n \approx \frac{g\tau k\Delta x}{|n|_{(v_{gr}=0)}} > \frac{g\tau k\Delta x}{g\tau} > \frac{g\tau k\Delta x}{|p|_{(v_{gr}=0)}} \approx \varphi_p. \quad (31)$$

Because the term in the center of this inequality ( $k\Delta x$ ) is the phase shift of the intensity grating it is clear that the electron distribution is ahead of the new intensity grating for  $\tau \ll t < \tau_{diel}$ . This is just the behavior found in Fig. 9 for  $v_{gr} \approx (k\tau_{diel})^{-1}$ .

From the electron and hole amplitudes and their phases given in Figs. 7 and 9 we have again calculated the differences  $\gamma_{rel} = 2(|p| - |n|)/(|p| + |n|)$  and  $\Delta\varphi_{np}$ . These quantities are plotted in Fig. 10. As expected from the discussion above,  $\gamma_{rel}$  has its maximum for  $v_{gr} = 0$  and decreases with  $v_{gr}$  on a scale defined by  $(k\tau_{diel})^{-1}$ . The phase difference  $\Delta\varphi_{np}$  on the other hand is zero for  $v_{gr} = 0$  and has a maximum at around  $(k\tau_{diel})^{-1}$ . The fact that the maximum  $\Delta\varphi_{np}$  is at a velocity defined by  $(k\tau_{diel})^{-1}$  is not restricted to the relaxation-time regime but was also observed in the lifetime regime (see Fig. 5). This can be verified by the analytical derivation of the velocity where  $\Delta\varphi_{np}$  has its maximum using Eq. (21).

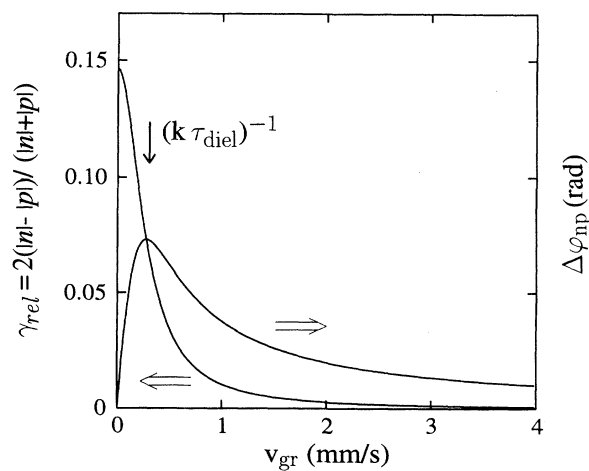


FIG. 10. Differences  $\gamma_{rel}$  (left scale) and  $\Delta\varphi_{np}$  (right scale) as a function of  $v_{gr}$  in the relaxation-time regime.

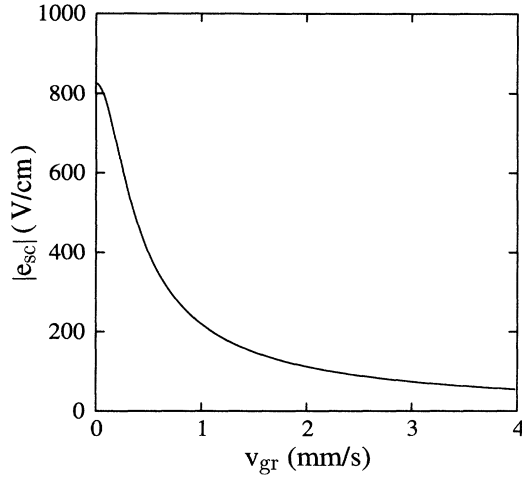


FIG. 11. Amplitude of the electric field as a function of  $v_{gr}$  in the relaxation-time regime.

We obtain

$$v_{(\Delta\varphi_{np}=\max)} = \frac{1}{k\tau_{\text{diel}}} \sqrt{1 + \frac{(b+1)^2 l^2}{2b} \frac{1}{a} + \frac{(b+1)^2 l^4}{4b} \frac{1}{a^2}}. \quad (32)$$

If the grating period  $\Lambda$  is chosen large enough,  $l$  becomes so small that the square root in Eq. (32) can be approximated by 1. Under this condition  $\Delta\varphi_{np}$  peaks at  $(k\tau_{\text{diel}})^{-1}$ . By inserting the parameters used for the analysis here into Eq. (32), we find that the corrections to  $(k\tau_{\text{diel}})^{-1}$  are  $\approx 10\%$  for the undoped sample (lifetime regime) and  $\approx 1\%$  for the doped sample (relaxation-time regime) [see also the arrows at  $(k\tau_{\text{diel}})^{-1}$  in Figs. 5 and 10]. Finally, we show in Fig. 11 the amplitude of the electric space charge field  $|e_{sc}|$  as a function of  $v_{gr}$  for the doped sample. It amounts to 800 V/cm for the nonmoving grating, i.e.,  $|e_{sc}|$  is five times higher than in the case of the undoped sample (compare Fig. 6), partly due to the higher generation rate.

### B. Short circuit current

The densities of photogenerated electrons and holes that exist due to the illumination by the moving intensity grating which were discussed in the preceding section are not directly accessible in our experiment. As mentioned in Sec. IV A, due to the phase shift between electron and hole densities a short circuit current results which is the quantity that we measure. The short circuit current density, as described by Eq. (26), is the ratio between one term that is proportional to  $v_{gr}$  and another term that is a sum of a constant plus a term proportional to  $v_{gr}^2$  plus a term proportional to  $v_{gr}^4$ . The function therefore increases linearly with  $v_{gr}$  for small values of  $v_{gr}$  and de-

creases proportional to  $v_{gr}^{-3}$  for sufficiently large velocities. Thus, a maximum in  $j_{sc}$  is implied at a finite  $v_{\max}$  that depends on the constants  $c_2, c_3$ , and  $c_4$ . Setting the derivative of  $j_{sc}(v_{gr})$  equal to zero we obtain for  $v_{\max}$ :

$$v_{\max} = \sqrt{\frac{-c_3 + c_3 \sqrt{1 + 12c_4 c_2 / c_3^2}}{6c_4}}. \quad (33)$$

Expanding the term  $\sqrt{1 + 12c_4 c_2 / c_3^2}$  into a power series we obtain for  $12c_4 c_2 / c_3^2 \ll 1$

$$v_{\max} \approx \sqrt{\frac{c_2}{c_3}} \approx \sqrt{\frac{a^2 \tau^{-2}}{k^2 (1 + a^2)}}. \quad (34)$$

According to Eq. (27) these approximations are valid if  $l \ll 1$ , i.e., if  $\Lambda$  is chosen sufficiently large compared to the ambipolar diffusion length  $\sqrt{D\tau}$ .

#### 1. Lifetime regime

In the lifetime regime ( $a \gg 1$ ) we can further approximate Eq. (34) and obtain

$$v_{\max} \approx (k\tau)^{-1}. \quad (35)$$

Under conditions where these approximations are valid the carrier recombination lifetime can be determined directly from the velocity corresponding to the maximum in the short circuit current. We have used this fact in order to measure the lifetime as a function of light intensity for  $a$ -Si:H (Ref. 15) in good agreement with conventional measurements of  $\tau$  by time resolved decay measurements of the photoconductivity.<sup>21</sup>

#### 2. Relaxation-time regime

If the dielectric relaxation time is large compared to  $\tau$  ( $a \ll 1$ ), Eq. (34) becomes

$$v_{\max} \approx (k\tau_{\text{diel}})^{-1} \quad (36)$$

and, thus,  $v_{\max}$  is determined merely by  $\tau_{\text{diel}}$ , i.e., by the photoconductivity of the sample. This was already clear from Eq. (32) because the peak in  $\Delta\varphi_{np}$  implies a peak in  $j_{sc}$  according to Eq. (25). Note that the velocity dependence of the product  $|n||p|$  that enters into Eq. (25) gives only minor corrections to the peak position in the relaxation-time regime for  $v_{gr} \approx (k\tau_{\text{diel}})^{-1}$  (see Fig. 7).

#### 3. Dependence of $v_{\max}$ on $\tau/\tau_{\text{diel}}$

In order to check the validity of the approximations made for  $v_{\max}$  in the two regimes, we display  $(v_{\max} k)^{-1}$  as a function of  $\tau_{\text{diel}}/\tau = a^{-1}$  in a log-log plot for a set of values of  $l$  in Fig. 12. In the lifetime regime (left-hand side of the figure)  $(v_{\max} k)^{-1}$  approaches  $\tau$ , if  $l < 0.1$ , i.e., Eq. (35) is valid.

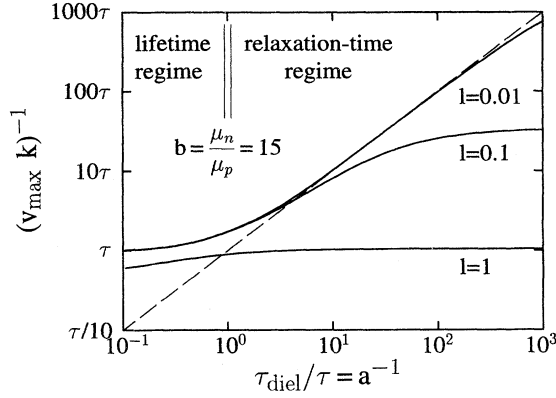


FIG. 12. Log-log plot of  $(v_{\max}k)^{-1}$  vs  $\tau_{\text{diel}}/\tau$  according to Eq. (33). Different curves correspond to different values of  $l$ . The ratio of electron to hole drift mobility  $b$  was chosen to be 15. The dashed line corresponds to the relationship  $(v_{\max}k)^{-1} = \tau_{\text{diel}}$ .

In the relaxation-time regime (right-hand side of the figure) the curves approach the relationship  $(v_{\max}k)^{-1} = \tau_{\text{diel}}$  (dashed line), if  $l$  is sufficiently small ( $l = 0.01$  for the range shown). This behavior is expressed in Eq. (36).

## V. EVALUATION OF EXPERIMENTAL DATA

In this section we show how the material parameters  $\mu_n$ ,  $\mu_p$ , and  $\tau$  are obtained by fitting the measured short circuit current to the theoretical expression given by Eq. (26). We do this in the next two sections for two samples for which the conditions of the lifetime regime and the relaxation-time regime are fulfilled, respectively.

### A. Lifetime regime: undoped *a*-Si:H measured at room temperature

For the undoped sample the photoconductivity when plotted versus light intensity follows a power law with exponent 0.78. This implies that the majority mobility lifetime product  $\mu_n\tau$  depends on the light intensity (i.e.,  $\mu_n\tau \propto I_0^{-0.22}$ ). Hence, we performed all measurements discussed here at a fixed intensity  $I_0 = 10 \text{ mW/cm}^2$  by changing the grating period  $\Lambda$  only. The short circuit currents measured for  $\Lambda = 3 \mu\text{m}$  as a function of  $v_{\text{gr}}$  are plotted in Fig. 13 as circles. The short circuit current is zero for  $v_{\text{gr}} = 0$  and increases linearly for small values of  $v_{\text{gr}}$ . After reaching a maximum for  $v_{\text{gr}}$  around 0.25 m/s,  $j_{\text{sc}}$  decreases steadily up to  $v_{\text{gr}} = 3 \text{ m/s}$ , the highest velocity used, in agreement with the discussion of Eq. (26) given above. Also shown in the figure is the best theoretical approximation to the measurements via Eq. (26) that was obtained by varying  $\mu_n$ ,  $\mu_p$ , and  $\tau$  and using the experimentally determined generation rate  $G_0 = 1.8 \times 10^{20} \text{ cm}^{-3} \text{ s}^{-1}$  and a modulation ratio of  $g/G_0 = 0.5$ . For better comparison of the exper-

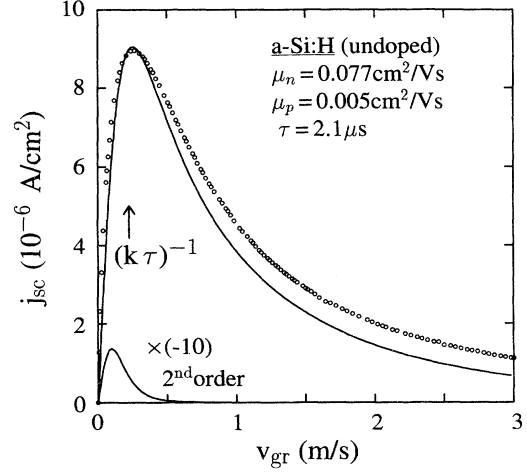


FIG. 13. Undoped *a*-Si:H: Short circuit current density measured with the setup of Fig. 1 as a function of  $v_{\text{gr}}$ . The measured data are shown as circles. The upper solid curve is the best fit using the analytical expression derived in Sec. III [Eq. (26)], corresponding to the material parameters given in the figure. Experimental data were normalized to the maximum by multiplication by 1.24. Also shown is the theoretical curve of the second order contributions  $j_{\text{sc},2}$  [Eq. (A1)] as calculated in the Appendix. Note the different scaling.

imental and theoretical curve shapes we have normalized both curves to the same maximum. For that purpose the experimental values were multiplied with 1.24. The values for  $\mu_n$ ,  $\mu_p$ , and  $\tau$  given in Fig. 13 fit not only the data for  $\Lambda = 3 \mu\text{m}$  best but also a complete set of measurements with different grating periods between  $0.4 \mu\text{m} \leq \Lambda \leq 9 \mu\text{m}$ .

The maximum short circuit current  $j_{\text{sc,max}}$  measured for each grating period is compared in Fig. 14 with the

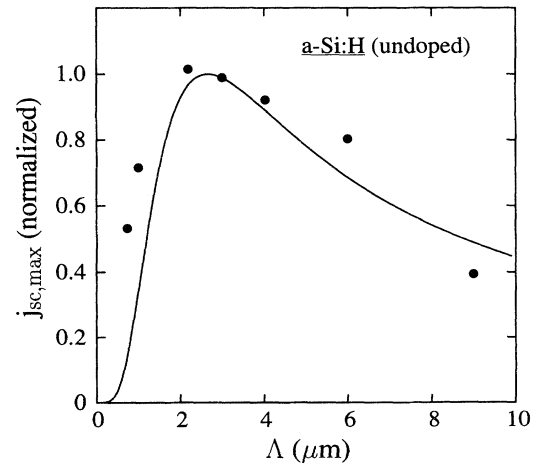


FIG. 14. Undoped *a*-Si:H: Maximum short circuit current as a function of grating period  $\Lambda$ . Dots are measured data and the solid curve is the theoretical expression obtained by using the material parameters of Fig. 13.

theoretical current densities that are obtained by inserting  $v_{\max}$  [Eq. (33)] into the formula for  $j_{sc}$ . The two sets of data have again been normalized by using the same normalization factor of 1.24 that was used for Fig. 13. The theoretical function reproduces the measured values of  $j_{sc,\max}$  reasonably well; note that the curve was calculated by inserting the material parameters that were obtained by fitting the curve shapes  $j_{sc}(v_{gr})$  for all values of  $\Lambda$ , only; i.e.,  $\mu_n$ ,  $\mu_p$ , and  $\tau$  have not been further adjusted to get the agreement shown in Fig. 14.

We estimate the accuracy of the fitting parameters to be 10% for  $\tau$ , 30% for  $\mu_n$ , and  $b = \mu_n/\mu_p$  to lie between 10 and 25. If parameters outside the range given above are chosen, the measured data are no longer reproduced. The material parameters obtained for  $I_0 = 10 \text{ mW/cm}^2$  are summarized here for undoped *a*-Si:H

$$\tau = 2.1 \times 10^{-6} \text{ s} \quad (\pm 0.2 \times 10^{-6} \text{ s}),$$

$$\mu_n = 0.077 \text{ cm}^2/\text{V s} \quad (\pm 0.02 \text{ cm}^2/\text{V s}),$$

$$\mu_p = 0.005 \text{ cm}^2/\text{V s}$$

$$(0.002 \text{ cm}^2/\text{V s} \leq \mu_p \leq 0.01 \text{ cm}^2/\text{V s}).$$

For an independent check we calculate the photoconductivity by inserting the material parameters obtained by the moving-photocurrent-grating experiment into

$$\sigma_{ph} = G_0 \tau e (\mu_n + \mu_p)$$

and obtain  $\sigma_{ph} = 4.9 \times 10^{-6} \Omega^{-1} \text{ cm}^{-1}$ . The photoconductivity that we measure for an externally applied voltage of 1 V is  $2.4 \times 10^{-6} \Omega^{-1} \text{ cm}^{-1}$  which is in reasonable agreement.

### B. Relaxation-time regime: *n*-type doped *a*-Si:H measured at 120 K

For the theory described in Sec. III to hold,  $N_0 = P_0$  was assumed, which requires that the density of thermally excited electrons and holes has to be well below that of photogenerated electrons and holes, respectively. This criterion was not met for the *n*-type doped sample where the photoconductivity at room temperature was no longer large compared to the dark conductivity. However, at 120 K this criterion was fulfilled. The photoconductivity for that sample at 120 K using  $I_0 = 80 \text{ mW/cm}^2$  was  $\sigma_{ph} = 4.4 \times 10^{-9} \Omega^{-1} \text{ cm}^{-1}$ . This is around 500 times smaller than  $\sigma_{ph}$  for the undoped sample at room temperature, implying that  $\tau_{\text{diel}}$  in turn is 500 times larger ( $\tau_{\text{diel}} = 2.4 \times 10^{-4} \text{ s}$ ). If the lifetime does not differ significantly for the two samples we are dealing with the relaxation-time regime in this case, an expectation that is borne out by the analysis below.

We observed a linear relationship between the photoconductivity and the light intensity, i.e., the majority carrier mobility lifetime product  $\mu_n \tau$  is constant. We measured the short circuit current as a function of grating velocity for a grating period  $\Lambda = 0.4 \mu\text{m}$  and for two light intensities ( $I_0 = 80 \text{ mW/cm}^2$  and  $240 \text{ mW/cm}^2$ , respectively). The data are shown in Fig. 15 together with

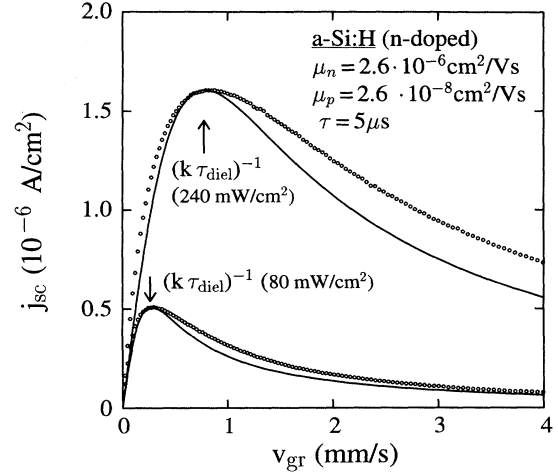


FIG. 15. Doped *a*-Si:H at 120 K: Experimental and theoretical short circuit current densities as a function of  $v_{gr}$  for two light intensities (lower curve:  $I_0 = 80 \text{ mW/cm}^2$ ; upper curve:  $I_0 = 240 \text{ mW/cm}^2$ ). For better comparison of the curve shape, experimental data were normalized to the theoretical curve at its maximum by multiplication by 1.05 and 1.15 for 80 and 240  $\text{mW/cm}^2$ , respectively.

the respective theoretical curves calculated using Eq. (26). Both sets of experimental data are fitted using the same set of material parameters  $\mu_n = 2.6 \times 10^{-6} \text{ cm}^2/\text{V s}$ ,  $\mu_p = \mu_n/100$ , and  $\tau = 5 \times 10^{-6} \text{ s}$  with the different generation rates inserted into Eq. (26). Thus it appears that not only the  $\mu\tau$  product but also  $\mu$  and  $\tau$  separately are independent of the light intensity for this sample.

The photoconductivity calculated from the material parameters given above and from the generation rate for  $I_0 = 80 \text{ mW/cm}^2$  is  $\sigma_{ph} = 4.2 \times 10^{-9} \Omega^{-1} \text{ cm}^{-1}$ . This good agreement with the measured photoconductivity given above can be considered as a check of the correct evaluation of the MPG technique in the relaxation-time regime.

## VI. CONCLUSION

In this paper we have discussed physical mechanisms that underlie the moving-photocurrent-grating technique for the determination of the lifetime and the mobilities of photogenerated electrons and holes in semiconductors. The intensity pattern used for the generation of photocarriers is obtained by the superposition of two frequency shifted laser beams yielding an intensity that depends sinusoidally on space and time. As a result of the different diffusion coefficients for electrons and holes space charges build up that result in a modulated internal electric field. This field acts on the photocarriers resulting in a short circuit current, the quantity that we measure in our experiment as a function of grating velocity and period. Fitting experimental data for amorphous hydrogenated silicon by the analytical expression for the short circuit current derived in this paper we determine  $\mu_n$ ,  $\mu_p$ , and  $\tau$ .

The result is in good agreement with the  $\mu\tau$  product deduced from the photoconductivity measured at the same light intensity, a fact that gives us confidence in our evaluation of the MPG technique.

The advantage of the MPG method is that it does not require complementary data as time or frequency resolved conductivity measurements in order to obtain a complete set of material parameters. We want to emphasize here that, although temporal information is obtained from our experiment, the measured quantity is a dc quantity simplifying the setup for the electronic measurement considerably.

#### ACKNOWLEDGMENTS

We thank C. Witt for valuable discussions and critical reading of the manuscript. This work was supported by the Deutsche Forschungsgemeinschaft under Project No. LE634/4-1-126193.

#### APPENDIX A: HIGHER ORDER CORRECTIONS TO THE SHORT CIRCUIT CURRENT

For the experiments a modulation ratio of the order of  $g/G_0=0.5$  was used. Since this ratio is not small compared with unity, the application of the small signal approximation might be questioned. In order to estimate the corrections from the first order theory described in Sec. III we include second harmonic terms, i.e., those with spatial period  $\Lambda/2$ . The inclusion of these terms into Eqs. (12) and (13) and the calculation of the second order correction to the short circuit current density  $j_{sc,2}$  along the line of calculations of Sec. III yields the following expression:

$$j_{sc,2}(k, v_{gr}) = \frac{c'_1 v_{gr} + c''_1 v_{gr}^3}{(c'_2 + c'_3 v_{gr}^2 + c'_4 v_{gr}^4)(c_2 + c_3 v_{gr}^2 + c_4 v_{gr}^4)^2}, \quad (\text{A1})$$

where

$$c'_1 = -\frac{g^4 e^4 k^4 \tau^6}{2(\epsilon\epsilon_0)^3} (\mu_n + \mu_p)(D_n - D_p)^2 \left\{ [12\mu_n \mu_p D_n D_p (D_n - D_p)] k^6 \right. \\ \left. + \left[ \mu_n \mu_p [14\mu_n D_p + 4(\mu_n D_n + \mu_p D_p)] (D_n - D_p) \frac{eN_0}{\epsilon\epsilon_0} + 2\mu_n \mu_p (D_n^2 - D_p^2) \frac{1}{2\tau} \right] k^4 \right. \\ \left. + \left[ 5\mu_n \mu_p (\mu_n + \mu_p)^2 (D_n - D_p) \frac{e^2 N_0^2}{(\epsilon\epsilon_0)^2} + (\mu_n^3 D_p - \mu_p^3 D_n) \frac{3eN_0}{2\tau\epsilon\epsilon_0} \right] k^2 + (\mu_n - \mu_p)(\mu_n + \mu_p)^3 \frac{e^2 N_0^2}{2\tau(\epsilon\epsilon_0)^2} \right\}, \quad (\text{A2})$$

$$c''_1 = -\frac{g^4 e^4 k^4 \tau^6}{2(\epsilon\epsilon_0)^3} (\mu_n + \mu_p)(D_n - D_p)^2 \left\{ 6\mu_n \mu_p (D_n - D_p) k^4 + \frac{1}{2\tau} (\mu_n^2 - \mu_p^2) k^2 \right\}, \quad (\text{A3})$$

and where the constants  $c_2$ ,  $c_3$ , and  $c_4$  are those defined in Eq. (27), whereas  $c'_2$ ,  $c'_3$ , and  $c'_4$  are obtained by substituting  $k$  by  $2k$  and  $l$  by  $2l$  in Eq. (27) for  $c_2$ ,  $c_3$ , and  $c_4$ , respectively.

For the undoped sample we have inserted the material parameters as obtained in Sec. V into Eq. (A1) and obtained the plot of  $j_{sc,2}(v_{gr})$  shown in Fig. 13 as the lower curve. For clarity  $j_{sc,2}$  was multiplied by  $-10$ . It can be seen that these corrections are negative and only in the percent range. For the doped sample higher order corrections are even less important.

- <sup>1</sup> J. R. Haynes and W. Shockley, Phys. Rev. **81**, 835 (1951).
- <sup>2</sup> D. Ritter, E. Zeldov, and K. Weiser, Appl. Phys. Lett. **49**, 791 (1986).
- <sup>3</sup> D. Ritter, E. Zeldov, and K. Weiser, J. Appl. Phys. **62**, 4563 (1987).
- <sup>4</sup> I. Balberg, J. Appl. Phys. **67**, 6329 (1990).
- <sup>5</sup> E. Sauvin, J. Hubin, A. Shah, and P. Pipoz, Philos. Mag. Lett. **63**, 327 (1991).
- <sup>6</sup> C. D. Abel and G. Bauer, in *Amorphous Silicon Technology—1992*, edited by M. J. Thompson, Y. Hamakawa, P. G. LeComber, A. Madan, and E. A. Schiff, MRS Symposia Proceedings No. 258 (Materials Research Society, Pittsburgh, 1992), p. 705.
- <sup>7</sup> F. Wang and R. Schwarz, J. Appl. Phys. **71**, 791 (1992).
- <sup>8</sup> D. Ritter, E. Zeldov, and K. Weiser, Phys. Rev. B **38**, 8296 (1988).
- <sup>9</sup> S. C. Moss, J. R. Lindle, H. J. Mackey, and A. L. Smirl, Appl. Phys. Lett. **39**, 227 (1981).
- <sup>10</sup> K. Hattori, T. Mori, H. Okamoto, and Y. Hamakawa, Appl. Phys. Lett. **51**, 1259 (1987).
- <sup>11</sup> K. Hattori, Y. Koji, S. Fukuda, W. Ma, H. Okamoto, and

- Y. Hamakawa, J. Appl. Phys. **73**, 3846 (1993).
- <sup>12</sup> U. Haken, M. Hundhausen, and L. Ley, J. Non-Cryst. Solids **164-166**, 497 (1993).
- <sup>13</sup> U. Haken, M. Hundhausen, and L. Ley, Appl. Phys. Lett. **63**, 3066 (1993).
- <sup>14</sup> G. S. Trofimov and S. I. Stepanov, Sov. Phys. Solid State **28**, 1559 (1986).
- <sup>15</sup> C. Witt, U. Haken, and M. Hundhausen, Jpn. J. Appl. Phys. **33**, L1809 (1994).
- <sup>16</sup> D. L. Staebler and C. R. Wronski, Appl. Phys. Lett. **31**, 292 (1977).
- <sup>17</sup> Y. M. Li, Phys. Rev. B **42**, 9025 (1990).
- <sup>18</sup> K. Hattori, H. Okamoto, and Y. Hamakawa, Phys. Rev. B **45**, 1126 (1992).
- <sup>19</sup> A. R. Moore, in *Semiconductors and Semimetals*, edited by J. I. Pankove (Academic, New York, 1984), Vol. 21, Pt. C, pp. 239–256.
- <sup>20</sup> R. A. Smith, *Semiconductors* (Cambridge University Press, Cambridge, 1969), p. 172.
- <sup>21</sup> M. Haridim, M. Zelikson, and K. Weiser, Phys. Rev. B **49**, 13 394 (1994).